Submitted to *Scripta Materialia*, July 2017. Revised September 2017.

# Fabricating geometrically-complex $B_4C$ ceramic components by robocasting and pressureless spark plasma sintering

**Siamak Eqtesadi [a], Azadeh Motealleh [a], Fidel H. Perera [b], Pedro Miranda [b], Antonia Pajares [b], Rune Wendelbo [a], Fernando Guiberteau [b], and Angel L. Ortiz [b],***

[a] Abalonyx AS, Oslo, Norway

[b] Department of Mechanical, Energy, and Materials Engineering,
University of Extremadura, 06006 Badajoz, Spain

## Abstract

Robocasting and pressureless spark plasma sintering are combined for the first time to fabricate geometrically-complex $B_4C$ components. It is shown that robocasting allows $B_4C$ green pieces to be printed with near-net shape from inks with suitable rheological properties, and that subsequent pressureless spark plasma sintering permits an ultrafast, energy-efficient, solid-state densification that yields $B_4C$ parts with adequate mechanical properties. Furthermore, the usefulness of cold-isostatic pressing to improve the densification of the pieces is evaluated, and the benefits of robocasting over conventional dry powder compaction are identified. Finally, the scalability for the production of large $B_4C$ pieces is discussed.

**Keywords:** $B_4C$; robocasting; pressureless spark plasma sintering; complex-shaped parts.

* Corresponding author:
Angel L. Ortiz
Phone: +34 924289600 Ext: 86726
Fax: +34 924289601
E-mail: **alortiz@unex.es**

Fabricating geometrically-complex ceramic articles with near-net shape is a long-sought objective of the ceramic industry with a view to reducing, and ideally to eliminating, the production costs associated with the post-sintering machining and finishing operations required to extract complex shapes from pieces with simple geometries. The motivation soars for ultra-hard ceramics because these operations can become prohibitively expensive and time-consuming, even inviable in some cases. $B_4C$, also known as black diamond, is one of these super-hard and ultralight engineering ceramics demanded at the industrial scale in parts with complex geometries. For example, one $B_4C$ application receiving great attention today is that of personnel and vehicle armour components [1-4]. The former must have ergonomic designs to protect body zones with different curvatures without penalizing mobility, and the latter custom designs to offer maximal coverage of the chassis or fuselage without jeopardizing maneuverability. Another major application of $B_4C$ is in tribocomponents [1,2,5] such as nozzles for blasting and water-jet cutting, cutting tools and dies, and other wear-resistant parts.

The near-net shape fabrication of a geometrically-complex ceramic article entails the shaping of the corresponding green compact (normally by any wet or plastic forming method), followed by its pressureless sintering. Unfortunately however, $B_4C$ is hardly densifiable in the pure state by conventional pressureless solid-state sintering [2]. Thus, hot-pressing is the reference sintering technique for the consolidation of pure $B_4C$ powders into dense pieces [2]. The undesirable consequence is then that the external uniaxial pressure and the confinement in the die limit the production to simple geometries. Spark plasma sintering with pressure has the same limitations, and hot-isostatic pressing is intrinsically problematic (glass encapsulation problems) and therefore is used rather as a post-sintering complement [2]. Thus, there is a real need to develop routes enabling the production of near-net shaped $B_4C$ parts by the combination of innovative forming and sintering techniques.

In this context, additive manufacturing techniques have opened new doors for preparing ceramic green articles with complex shapes that are hardly or not-at-all manufacturable by traditional ceramic processes. Robocasting (RC) is a unique additive manufacturing method particularly well-suited to 3D-printing ceramic pieces. Green parts are built by extruding highly-concentrated aqueous suspensions (inks) of the desired ceramic powders through a fine nozzle. A robotic system moves the nozzle following a computer-aided design (CAD) model in order to build the part layer by layer [6,7]. Meanwhile, electric current activated or assisted sintering (ECAS) techniques have revolutionized the science of ceramic processing in general, especially for these hard-to-sinter ceramics. Pressureless spark plasma sintering (PSPS) is one of these novel ECAS techniques, consisting of the repeated application of high energy, low voltage, pulsed direct electrical current [8,9], without the help of external pressure. This combination of features enables the ultra-fast and energy-efficient densification of geometrically-complex ceramic green parts.

Given the above, it seemed that it could be worth exploring the combination of RC with PSPS as a solution to the problem of fabricating geometrically-complex $B_4C$ components with near-net shape. This study was aimed in this direction, to address two of the eight challenges [10] with societal import recently identified by the ceramic community: (i) ceramic processing through programmable design and assembly (*i.e.*, additive manufacturing, and RC in particular), and (ii) ceramics for extreme environments (including specifically tribological, super-abrasive, and armour materials).

With this idea in mind, we prepared an ink with 40 vol.% $B_4C$ loading and minimal organic content as follows. First, 1 wt.% (relative to $B_4C$ content) of a synthetic polyelectrolyte dispersant (Produkt KV5088, Zschimmer-Schwarz) was dissolved in deionized water at room temperature and natural pH, and the solution was agitated (ARE-250, Thinky) for 10 min at 700 rpm. Second, the $B_4C$ powder (Grade HD 20, H.C. Starck; $d_{10}$ ~0.1–0.36 μm, $d_{50}$ ~0.3–0.6 μm, and $d_{90}$ ~0.9–1.5 μm) was added in batches to this aqueous solution, each time agitating the resulting suspension for 10 min at 800 rpm. Third, 7 mg/mL (in the final suspension) of methylcellulose (Methocel F4M, $M_w$= 3500 g/mol, 5 wt.%; Dow Chemical Company) was introduced to viscosify the suspension, which was agitated for 10 min at 1000 rpm. Fourth, 4 vol.% (relative to liquid content) of polyethylenimine (PEI) flocculant (10% w/v in water, Sigma-Aldrich) was added to gellify the suspension. And fifth, the resulting colloidal ink was homogenized by agitation for 2 min at 1200 rpm followed by 7 min at 700 rpm.

Fig. 1 shows representative rheological properties of the $B_4C$ ink developed, measured using a rheometer (Discovery HR-2, TA Instruments Ltd.) configured in the parallel plate geometry (40 mm, and gap of 800 μm), demonstrating its suitability for RC. Specifically, it is seen in Fig. 1A that the ink has the shear-thinning flow behavior desirable for its extrusion as a smooth filament without die swell. Moreover, it is seen in Fig. 1B that the ink also exhibits a linear viscoelastic response at low stress with high values of stiffness (~2.5 MPa) and yield strength (~50–60 Pa, corresponding to the onset of the sudden fall), as required for the extruded filament to retain its form and support the weight of the layers above. $B_4C$ inks were formulated before using only PEI as both dispersant and binder and evaluated in terms of their rheological behaviour and printability [11]. Compared to that work, the ink prepared here exhibits a storage modulus two orders of magnitude higher, which in principle makes it more suitable for producing parts with overhanging features or internal holes/gaps.

Fig. 2 shows optical images confirming the feasibility of obtaining geometrically-complex $B_4C$ green articles by RC from this ink. We have printed different bulk and porous parts covering some typical $B_4C$ applications (Figs. 2A-B). They include square and hexagonal plates to build multi-segmented armour panels, gears of different sizes and morphologies for tribological applications, conical nozzles with various dimensions and tip sizes for blasting and water-jet cutting, and square and cylindrical porous elements for application as filters or catalytic supports. In all cases, 3D printing (A3200, 3D inks) was done under ambient deposition conditions using a conical nozzle (410 μm tip diameter, *d*) and a constant printing speed of 20 mm/s (corresponding to a flow rate of ~2.64 $mm^3/s$). Most pieces were printed using a parallel raster pattern with 342 μm (*d*/1.2) rod spacing, 356 μm (*d*/1.15) layer height, and 205 μm (*d*/2) in-plane shifting between adjacent layers, which yields a hexagonal stacking of filaments (close packed design; Fig. 2C) with optimal overlap, minimal excess ink overflow and without periodic, inter-rod defects [12]. Conical pieces were printed using a circular raster pattern comprising 3 concentric rings with the same rod spacing and layer height as before, but variable in-plane layer shifting depending on the desired cone angle. Porous $B_4C$ elements were printed adopting a tetragonal mesh with 820 μm (2*d*) rod spacing and 328 μm (*d*/1.2) layer height. As-printed parts were then dried for 48 h, yielding robust bulk green parts which, relative to the CAD model, shrank laterally and vertically by ~3±1% and ~5±1% respectively, and by ~4±1% and ~7±1% if post-isopressed (~1–2% additional isotropic shrinkage with respect to the dried green part). These slight differences between in-plane and out-of-plane dimensions is not attributed to any anisotropy during drying but rather to a minimal shape distortion occurring during printing due to both gravity and lateral overflow of excess ink. Nevertheless, if required to meet tolerances, this small shape deviation could be easily corrected by conveniently adjusting the initial CAD model dimensions.

As shown in Fig. 2D, the relative green density of as-dried robocast (RC) $B_4C$ bulk parts, measured on square plates from their mass and external dimensions, is ~53±2%, increasing up to ~58±2% with the subsequent cold-isostatic pressing (RC+CIP) at 200 MPa (which preserved shape). The reference cylindrical compacts prepared from the $B_4C$ powders by cold-uniaxial pressing (CP) at 50 MPa and by cold-uniaxial pressing at 50 MPa plus cold-isostatic pressing (CP+CIP) at 200 MPa have relative densities of ~45±1% and ~51±2% (~4±1% isotropic shrinkage with respect to the uniaxially-pressed compact), respectively. Therefore, the $B_4C$ parts shaped by RC have denser green microstructures than the articles shaped by conventional dry isostatic pressing (CP+CIP). This is attributable to the wet route favouring the sliding and rearrangement of the $B_4C$ faceted particles to a greater packing, but this observation does not imply generality.

Having demonstrated the versatility of RC in producing highly dense geometrically-complex $B_4C$ green parts, we next studied their pressureless spark plasma sinterability. The study was conducted on both as-robocast and post-isopressed green samples with square plate morphology to facilitate the subsequent measurements of density and shrinkage, with the cylindrical counterparts prepared by conventional dry pressing serving as reference baseline. PSPS was done (HP-D-10, FCT Systeme GmbH) in a dynamic vacuum (~3 Pa) at 1900, 2000, or 2100 °C for 5 min, using a heating ramp of 100 °C/min. A special graphite die assembly with circular geometry was used to avoid load application on the $B_4C$ pieces, which rested on the lower punch. Included in Fig. 2D are also the relative densities of all sintered pieces. As expected, the relative density of the robocast pieces (RC) increases from ~74±3 to 90±3% with increasing sintering temperature from 1900 to 2100 °C. Relative to CAD model, these pieces shrank laterally and vertically from ~9±1% and ~12±1% at 1900 °C up to ~17±1% and ~21±2% at 2100 °C, respectively. Therefore, within experimental errors, they seem to have shrunk isotropically during sintering (additional shrinkages of ~6–7% at 1900 °C and ~14–16% at 2100 °C). If isostatically pressed (RC+CIP), these pieces reach near-full densification (~95±3%) at 2100 °C, with total lateral and vertical shrinkages relative to the CAD model of ~20±2% and ~24±1%, respectively. Therefore, the isopressed pieces seem to have shrunk also isotropically during sintering (~16–17% additional shrinkage), thus preserving the shape of the corresponding green piece. This temperature is lower and the soaking time much shorter than typically required (several hours at ~2300 °C) for pure $B_4C$ powders to reach densifications greater than 90% by conventional pressureless solid-state sintering [2]. This result puts the advantages of PSPS into perspective –without any demerit to the major densification achieved in the green state by RC, especially when combined with CIP. Essentially, the ultrafast heating in PSPS allows high enough temperatures to be rapidly reached having eliminated the oxidic impurities, conditions at which densification is favored over coarsening. Interestingly, under identical sintering conditions, the pieces shaped by RC densified more (by ~6%) than their reference counterparts shaped by conventional dry pressing. This is attributable to the former having greater green-body densification –indeed, the same ~7–8% difference in density existed already in the green state. This same reason explains why robocast (RC) pieces reached essentially the same densification at 2000 °C as the uniaxial-pressed (CP) ones at 2100 °C. All these results confirm that shaping by RC is recommendable over the conventional dry-pressing route, at least for the particular $B_4C$ powder used.

The observations by scanning-electron microscopy (SEM; Quanta 3D FEG, FEI) of fracture surfaces created in $B_4C$ sintered pieces, such as those shown in Fig. 3, corroborate the deductions made from the density measurements. It is seen that the pieces shaped by RC are (i) very porous at 1900 °C, reaching only the early stage of the intermediate sintering regime (Fig. 3A), (ii) partially dense at 2000 °C, reaching the middle stage of the intermediate sintering regime (Fig. 3B), and (iii) very dense at 2100 °C, reaching the early stage of the final sintering regime (Fig. 3C). If isostatically pressed, the piece shaped by RC becomes near fully-dense at 2100 °C, reaching the later stage of the final sintering regime (Fig. 3D). Comparatively, at 2100 °C, the pieces shaped by dry uniaxial pressing (Fig. 3E) and by dry uniaxial+isostatic pressing (Fig. 3F) are only at the middle stage of the intermediate sintering regime and the later stage of the intermediate sintering regime, respectively.

Fig. 4 shows the hardness and compressive strength of the sintered $B_4C$ ceramics. The former was evaluated by Vickers indentation tests (MV-1, Matsuzawa) at 49 N load, and the latter was measured (on $3.2\times3.2\times5.5$ mm$^3$ parallelepipeds) by uniaxial compression tests (Hoytom 200kN, Hoytom S.L.) at a constant crosshead speed of 0.6 mm/min up to failure. In both cases the samples were placed with their printing plane (robocast ceramics) or their uniaxial-compaction plane (dry-pressed ceramics) perpendicular to the load axis. It is seen that both magnitudes increase (i) with increasing sintering temperature, and (ii) with the use of isostatic pressing, and that they are greater for the ceramics shaped by RC. Therefore, it is clear that both hardness and compressive strength correlate directly with the densification degree, increasing as the residual porosity decreases. The hardest and strongest of the present $B_4C$ ceramics (RC+CIP) has, despite its ~5% residual porosity, a hardness of ~27 GPa and a compressive strength of ~1800 MPa. This is an excellent combination of mechanical properties because $B_4C$ ceramics fabricated by conventional pressureless sintering have lower hardness values (18–24 GPa) [2], and the compressive strength is within the range (1400–3400 MPa) typically measured for $B_4C$ ceramics fabricated by hot-pressing [2]. Remarkably, the $B_4C$ ceramic shaped by RC only (without CIP) and then PSPS-ed at 2100 °C also exhibits, despite its ~10% residual porosity, hardness and compressive strength values in these intervals (~20.5 GPa and ~1450 MPa, respectively), which is not the case for any of the two $B_4C$ ceramics shaped by conventional dry-pressing techniques. Despite these outstanding results, there is still plenty of room for optimizing the proposed fabrication route –RC followed by PSPS, with or without an intervening CIP step– by tailoring the PSPS cycle. Future work in this direction (beyond the scope of this first proof-of-concept study) is expected to further reduce the residual porosity in the $B_4C$ ceramics, enabling them to reach super-high hardness and compressive strength values. Indeed, the hardness of $B_4C$ ceramics seems to increase exponentially with a rate constant of ~7 as the residual porosity decreases [13], so that hardness values as high as 35 GPa are anticipated for such dense $B_4C$ ceramics.

In conclusion, the present work demonstrates the feasibility of successfully fabricating geometrically-complex $B_4C$ ceramic parts with near-net shape and appropriate mechanical properties by combining RC with PSPS. This combination might have extensive practical implications, and may turn many what are now industrial aspirations for $B_4C$ into reality. In principle, the proposed processing route is scalable for the commercial production of large pieces given that there are already large RC devices and SPS units available on the market. PSPS is very energy efficient, which becomes especially important in the fabrication of large parts made from highly refractory ceramics. And for the sintering of large pieces, there exist SPS units equipped with inductive heating systems that prevent radial temperature gradients and with robotized systems that handle both placing the green parts in the chamber and extracting the sintered articles. The most limiting factor would be the printing times of large components in RC, but this can be conveniently adjusted without penalizing the dimensional accuracy by judicious control of the tip size and extrusion speed. Besides, the versatility of RC will directly enable curved or internally-complex pieces to be manufactured–if necessary, with the aid of fugitive inks that are to be eliminated before or during sintering [14]– and pieces with smoothly graded compositions can easily be built by using various ink dispersers and a mixing head.

This work was financially supported by the Ministerio de Economía y Competitividad (Government of Spain) under grant nº MAT2016-76638-R), and by the Junta de Extremadura under grants nº IB16094 and GR15078, all co-financed with FEDER Funds.

# References

1. F. Thevenot, J. Eur. Ceram. Soc. 6 (1990) 205–225.
2. A. Suri, C. Subramanian, J. Sonber, T. Murthy, Int. Mater. Rev. 55 (2010) 4–39.
3. S. Leo, C. Tallon, G.V. Franks, J. Am. Ceram. Soc. 97 (2014) 3013–3033.
4. V. Domnich, S. Reynaud, R.A. Haber, M. Chhowalla, J. Am. Ceram. Soc. 94 (2011) 3605–3628.
5. B.M. Moshtaghioun, D. Gomez-Garcia, A. Dominguez-Rodriguez, R.I. Todd, J. Eur. Ceram. Soc. 36 (2016) 3925–3928.
6. J.A. Lewis, J.E. Smay, J. Stuecker, J. Cesarano, J. Am. Ceram. Soc. 89 (2006) 3599–3609.
7. P. Miranda, E. Saiz, K. Gryn, A.P. Tomsia, Acta Biomater. 2 (2006) 457–466.
8. R. Orru, R. Licheri, A.M. Locci, A. Cincotti, G. Cao, Mat. Sci. Eng. R 63 (2009) 127–287.
9. Z.A. Munir, D.V. Quach, M. Ohyanagi, J. Am. Ceram. Soc. 94 (2011) 1–19.
10. K.T. Faber, T. Asefa, M. Backhaus-Ricoult, R.K. Brow, J. Chan, S. Dillon, W.G. Fahrenholtz, M.W. Finnis, J.E. Garay, E. Garcia, Y. Gogotsi, S.M. Haile, J.W. Halloran, J. Hu, L. Huang, S. Jacobsen, E. Lara-Curzio, J. LeBeau, W.E. Lee, C.G. Levi, I. Levin, J.A. Lewis, D.M. Lipkin, K. Lu, J. Luo, J.P. Maria, L.W. Martin, S. Martin, G.L. Messing, A. Navrotsky, N.P. Padture, C.A. Randall, G.S. Rohrer, A. Rozenflanz, T. Schaedler, D. Schlom, A. Sehirlioglu, A. Stevensen, T. Tani, V. Tikare, S. Trolier-McKinstry, H. Wang, and B. Yildiz, J. Am. Ceram. Soc. 100 [5] (2017) 1777–1803.
11. W.J. Costakis Jr., L.M. Rueschhoff, A.I. Diaz-Cano, J.P. Youngblood, R.W. Trice, J. Eur. Ceram. Soc. 36 (2016) 3249–3256.
12. E. Feilden, E. García-Tuñón, F. Giuliani, E. Saiz, L. Vandeperre, J. Eur. Ceram. Soc. 36 (2016) 2525–2533.

13. B.M. Moshtaghioun, D. Gomez-Garcia, A. Dominguez-Rodriguez, R.I. Todd, J. Eur. Ceram. Soc. 36 (2016) 1829–1834.

14. F.J. Martínez-Vázquez, A. Pajares, P. Miranda, J. Eur. Ceram. Soc (2017), under review.

## Figure Captions

**Figure 1.** Rheological characterization of the $B_4C$ ink used in the shaping by RC showing specifically the logarithmic plots of (A) viscosity *vs* shear rate and (B) storage modulus *vs* shear stress. Points are the experimental data, and the solid lines are just to guide the eye.

**Figure 2.** (A) Optical image captured *in situ* during the 3D printing of a geometrically-complex circular gear. (B) Optical images of several $B_4C$ green parts shaped by RC, and then dried. (C) View of a simple computer-aided design model showing the parallel raster pattern used. (D) Relative density (average of at least 3 measurements) of both the $B_4C$ green and the sintered parts for the different shaping procedures and sintering temperatures used.

**Figure 3.** SEM micrographs of fracture surfaces of the $B_4C$ sintered ceramics prepared under the pairs of shaping procedure–PSPS temperature indicated.

**Figure 4.** Vickers hardness and compressive strength of the $B_4C$ sintered parts for the different shaping procedures and sintering temperatures used.

**Figure(s)**

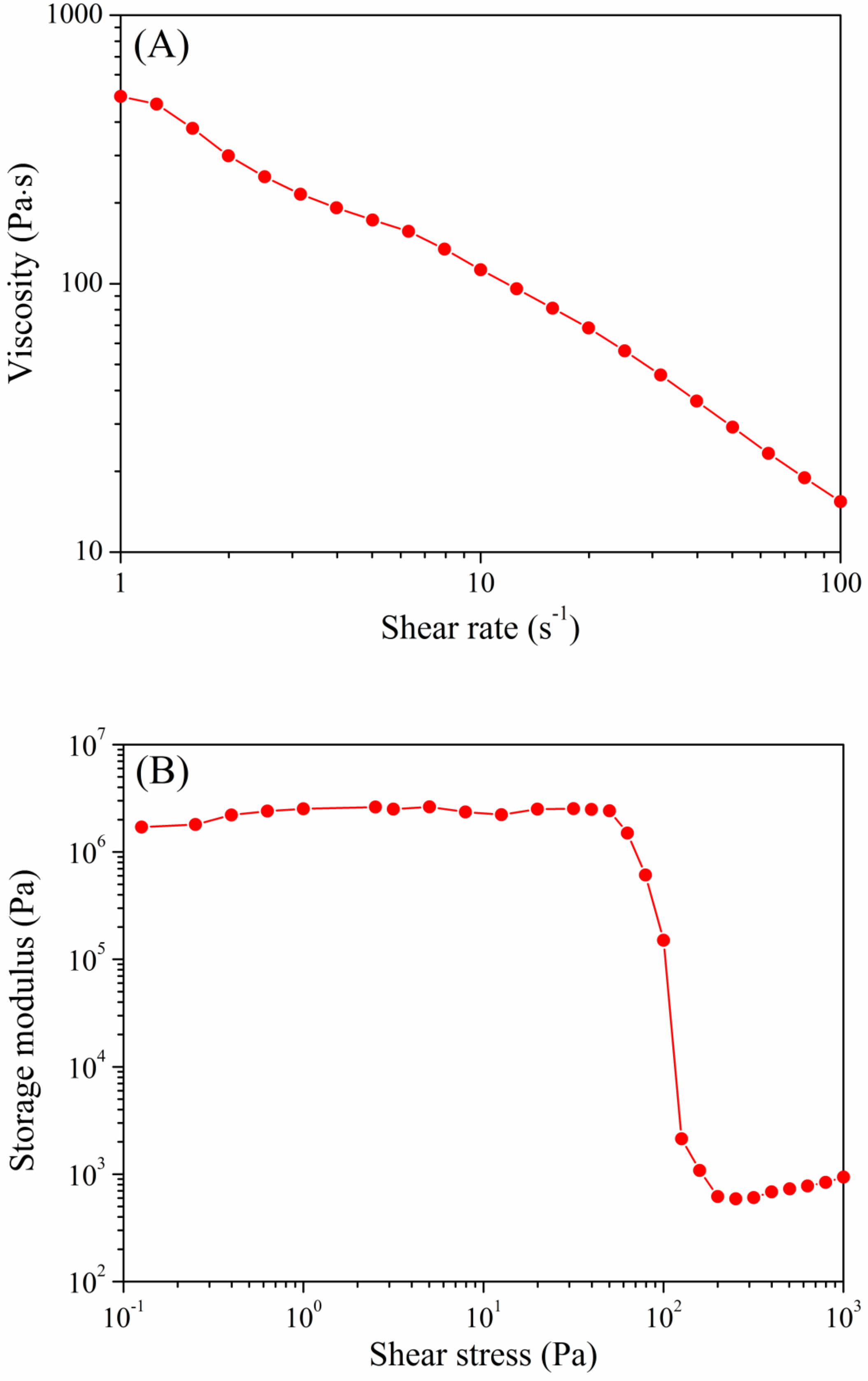

Eqtesadi *et al.*
Figure 1

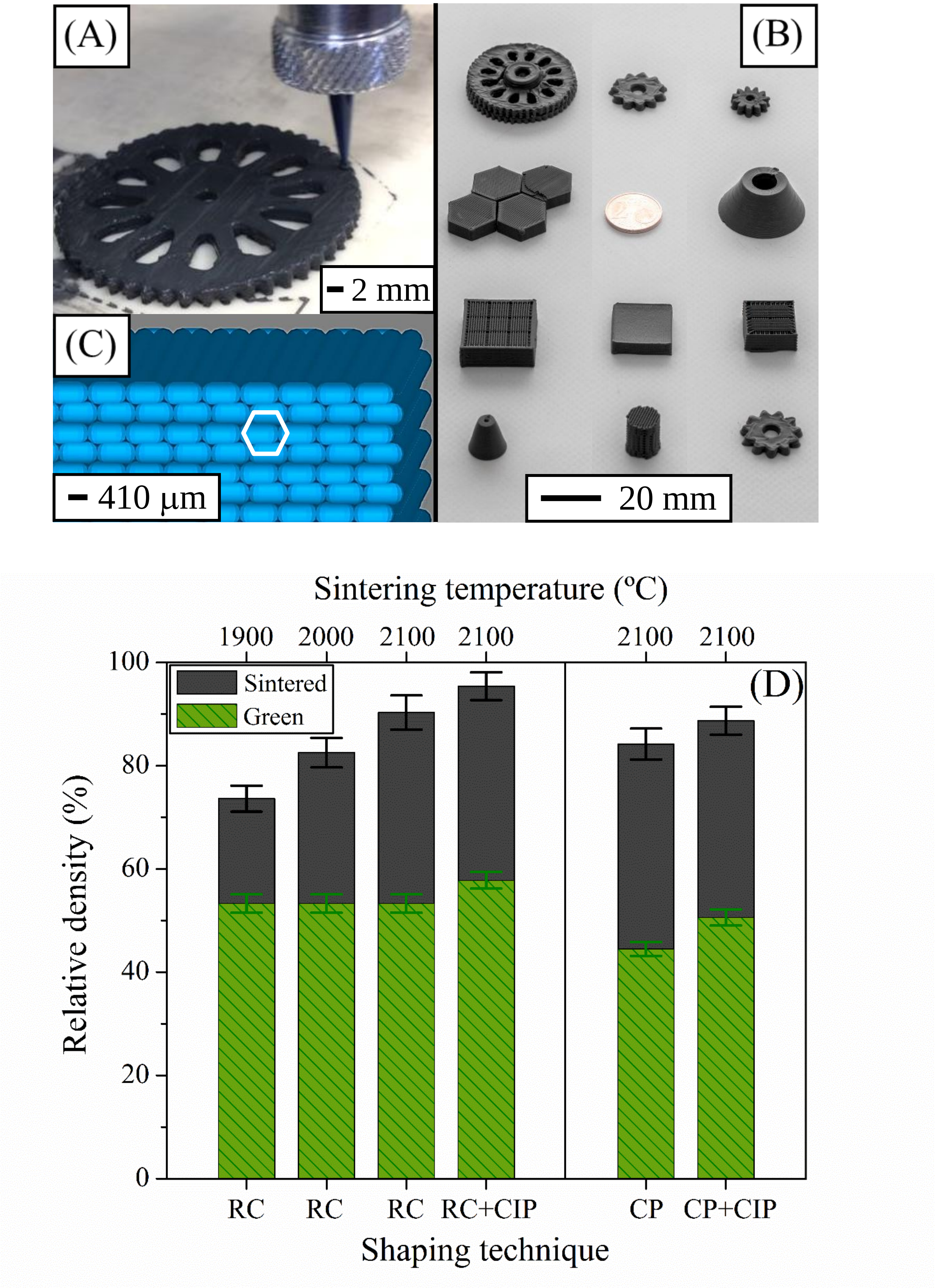

Eqtesadi *et al.*
Figure 2

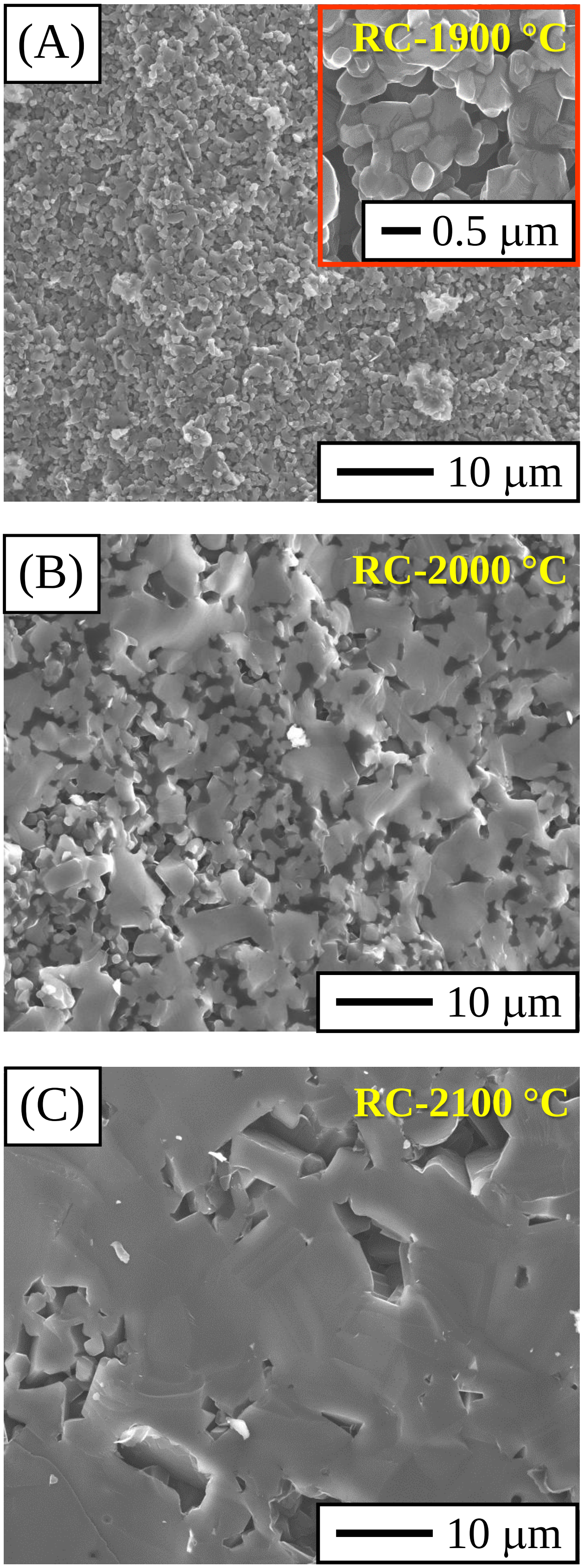

Eqtesadi *et al.*
Figure 3

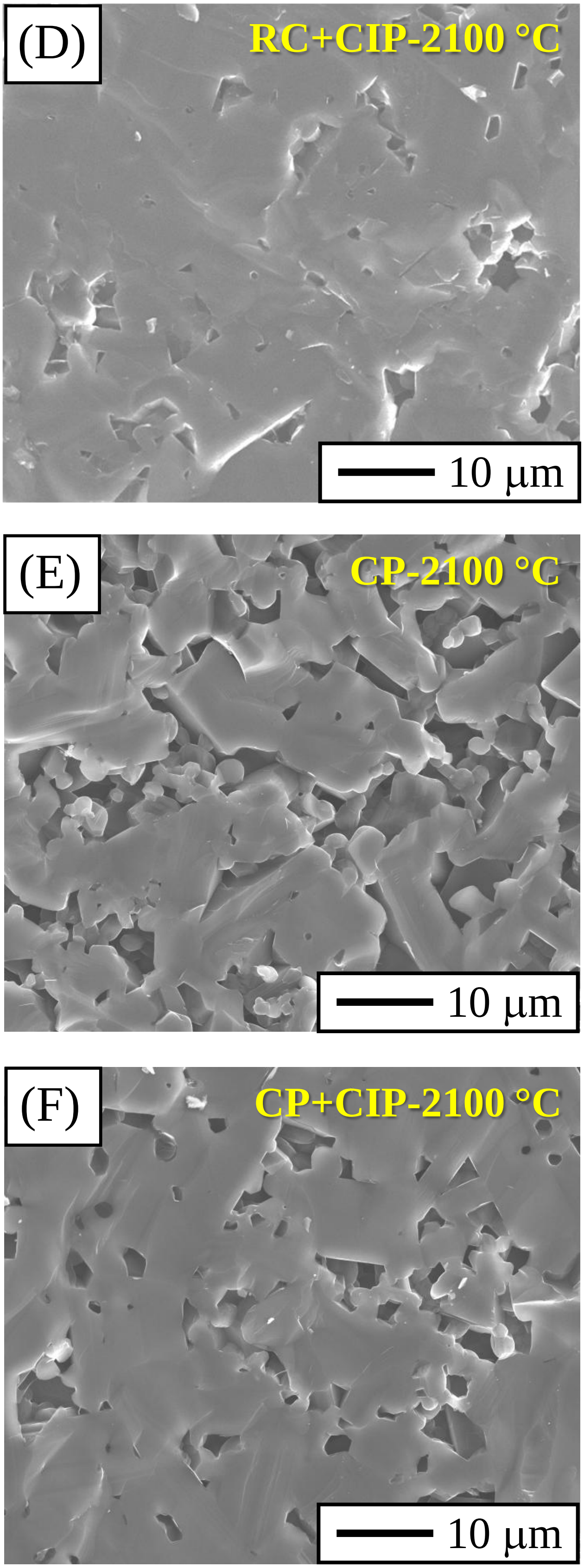

Eqtesadi *et al.*
Figure 3

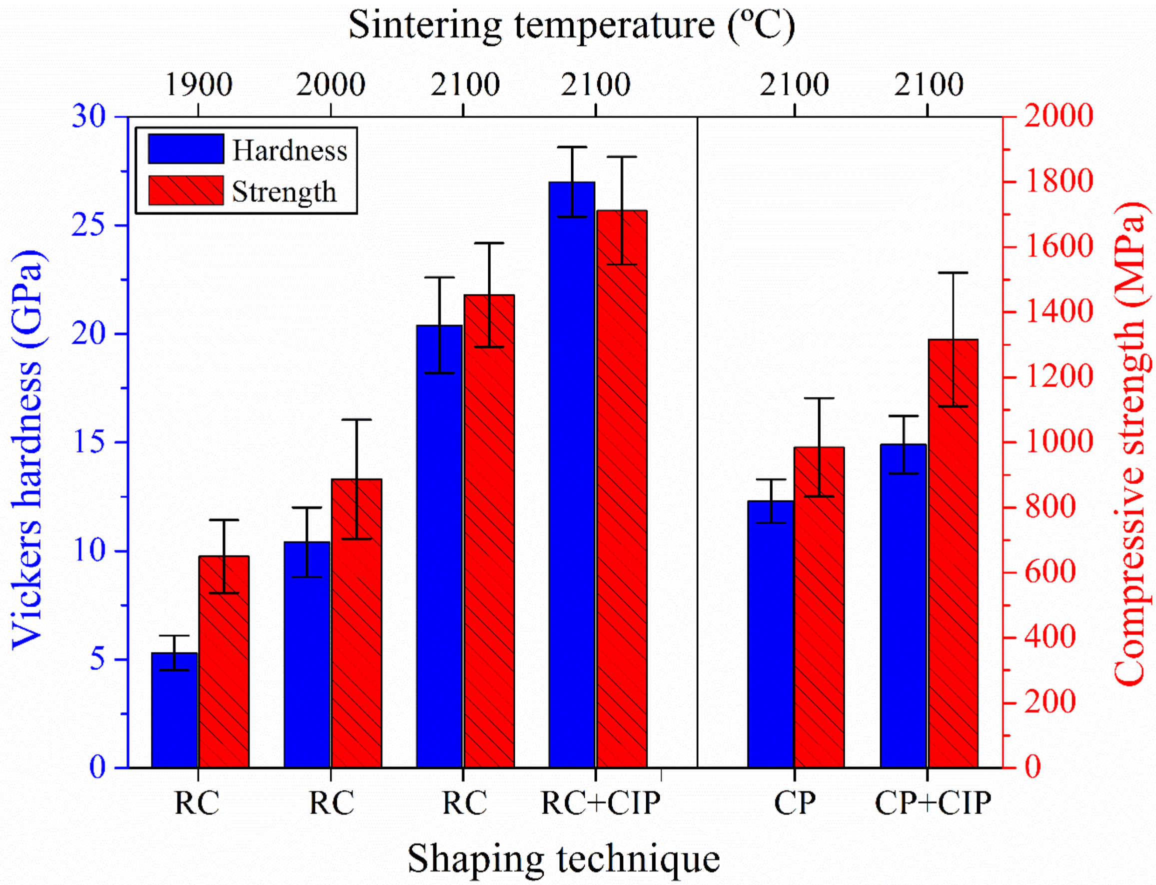

Eqtesadi *et al.*
Figure 4